PCCP

PAPER

View Article Online
View Journal | View Issue

Cite this: *Phys. Chem. Chem. Phys.*, 2016, **18**, 30323

Simulations of the water exchange dynamics of lanthanide ions in 1-ethyl-3-methylimidazolium ethyl sulfate ([EMIm][$EtSO_4$]) and water†

Yi-Jung Tu, Matthew J. Allen and G. Andrés Cisneros*

Received 16th July 2016,
Accepted 15th August 2016

DOI: 10.1039/c6cp04957e

www.rsc.org/pccp

The dynamics of ligand exchange on lanthanide ions is important for catalysis and organic reactions. Recent ^{17}O-NMR experiments have shown that water-exchange rates of lanthanide ions in water/1-ethyl-3-methylimidazolium ethyl sulfate (water/[EMIm][$EtSO_4$]) increase as a function of increasing charge density. The trend of water-exchange rates in this solvent is opposite to that observed in water. Since the lanthanide ions and ionic liquids investigated in that work were highly charged, an advanced polarizable potential is desirable for accurate simulations. To this end, we have developed atomic multipole optimized energetics for biomolecular applications (AMOEBA) parameters for all lanthanides and [EMIm][$EtSO_4$], and molecular dynamics simulations with the optimized parameters have been carried out to provide possible explanations for these observed behaviors from the experiments. In water, the association of a water molecule with the first hydration shell can lead to water exchange. Smaller lanthanide ions exhibit slower water-exchange rates than larger ones because they form smaller aqua complexes, preventing the binding of incoming water molecules from the outer hydration shells. By contrast, smaller lanthanide ions undergo faster water exchange in water/[EMIm][$EtSO_4$] because the dissociation of a water molecule is a key step for water-exchange events in this solvent. The first shell $[EtSO_4]^-$ anions bind closer to the smaller lanthanide ions, resulting in more steric crowding effects on the surrounding water and facilitating the release of water molecules.

Introduction

Lanthanides have been applied widely in lighting devices, medical diagnosis, catalysis and organic synthesis, because of their luminescent,[1–5] magnetic[6–9] and catalytic[10–13] properties. These properties can have a broad scope for modulation by altering the lanthanide ions and their coordination environments. Moreover, the interactions of lanthanide ions with solvents can influence solvent-exchange rates that are important for the efficiency of contrast agents for biomedical analysis, and catalysts in organic reactions.[14,15] Consequently, studies of the coordination chemistry and solvent exchange of lanthanide ions are of particular importance for the development of catalysis and other applications.

The application of room temperature ionic liquids has become popular in catalysis,[16–19] organic synthesis,[20,21] and separations.[22] In an effort to combine the advantages of lanthanide ions and ionic liquids, a number of properties of lanthanide ions in ionic liquids have been explored experimentally[1,6,10] and theoretically.[23,24] The properties of lanthanide ions in ionic liquids are often unique compared to those in conventional organic solvents.[1,6,10] However, to our knowledge, the solvent-exchange kinetics of lanthanide ions are studied mostly in aqueous and organic solvent systems.[25–33] Recently, the water-exchange rate of lanthanide ions in 1-ethyl-3-methylimidazolium ethylsulfate ([EMIm][$EtSO_4$]) was reported using ^{17}O-NMR spectroscopy to investigate the modulation of the kinetic properties of lanthanide ions in ionic liquids.[34] Those results revealed that the trend of water-exchange rates in [EMIm][$EtSO_4$] for different lanthanide ions is opposite to that observed in water. The water-exchange rates of lanthanide ions in [EMIm][$EtSO_4$] are also slower than those in water.

Theoretically, the factors that influence the structural and kinetic properties of lanthanide ions are mainly attributed to the electrostatic attractions between lanthanide ions and solvent molecules and to the electrostatic and steric repulsions between solvent molecules. The ligand field effect for lanthanide ions is small because of the shielding of 4f valence electrons by 5s and 5p electrons. However, the factors that control the rates

Department of Chemistry, Wayne State University, Detroit, Michigan, 48202, USA. E-mail: andres@unt.edu

† Electronic supplementary information (ESI) available: Definitions for all local frames, multipoles, and intra- and inter-molecular interactions of [EMIm][$EtSO_4$] and lanthanide–water dimers. MD simulation results for density and heat of vaporization, self-diffusion coefficients, and mean residence time. See DOI: 10.1039/c6cp04957e

and mechanisms of water-exchange on lanthanide ions in [EMIm][$EtSO_4$] were not clear and, thus, warranted further investigation.

Molecular dynamics (MD) simulations can provide useful structural and dynamic information on solvent-exchange processes.[23,24,28–30,35–37] However, an accurate force field is required for appropriately modeling intermolecular interactions among solvent molecules and electrostatic interactions between solvent molecules and lanthanide ions. Because the metal ions and the components of ionic liquids are highly charged ions, the force field for these species needs to be created. The Atomic Multipole Optimized Energetics for Biomolecular Applications (AMOEBA)[38] force field has been used to simulate hydration dynamics for various metal ions because it can accurately describe the interactions of metal ions with water molecules.[28,30,35–37,39] Recently, our group has incorporated Gaussian electrostatic model-distributed multipoles (GEM-DMs)[40] into the AMOEBA force field and was able to successfully estimate the bulk properties of imidazolium-based ionic liquids.[41]

In this paper, we develop AMOEBA force field parameters for lanthanide ions and the [EMIm][$EtSO_4$] ion pair. The resulting parameters were used to determine water-exchange rates in water and in water/[EMIm][$EtSO_4$]. The solvation characteristics, transport properties, and solvated structures from the MD trajectories were further examined to understand the contrasting water-exchange behaviors of lanthanide ions in these two solvent systems.

Methods

A. Parameterization of [EMIm][$EtSO_4$]

The procedure for the determination of the required AMOEBA parameters for ionic liquids has been described previously.[41] Briefly, this procedure involves the use of quantum mechanics (QM) energy decomposition analysis (EDA)[42] to determine and match individual inter-molecular interaction components for different dimers as well as employing the distributed multipoles obtained from the Gaussian electrostatic model-distributed multipole (GEM-DM)[40] method. The use of the GEM-DM parameters in AMOEBA force fields has been shown to provide accurate reproduction of a number of thermodynamic and transport properties of 1,3-dimethylimidazolium-based ionic liquids.[41] In this work, we follow the same fitting methodologies to develop intra- and inter-molecular parameters for the [EMIm][$EtSO_4$] ionic pair. All parameters have been optimized by comparison to the quantum calculations that included optimized structures, intermolecular interactions and energy decomposition analyses. To test the accuracy of the developed force field for [EMIm][$EtSO_4$], MD simulations were performed and compared with reported experimental densities[43] and heat vaporizations.[44,45] The parameters for the [EMIm][$EtSO_4$] ion pair are provided in the ESI.†

B. Parameterization of Gd^{3+}, Dy^{3+}, and Ho^{3+}

The AMOEBA parameters for the three lanthanide ions—Gd^{3+}, Dy^{3+}, and Ho^{3+}—were obtained by comparing energies calculated with the respective AMOEBA parameters with the interaction energies of lanthanide–water dimers obtained at the MP2 level[46–50] using the Gaussian software package.[51] Stuttgart's small core quasi-relativistic effective core potential and the associated basis sets[52–54] were used for the lanthanide ions, and 6-311G(d,p) basis sets were used for H and O atoms. The structures of mono aqua complexes for the three studied lanthanide ions were optimized and the intermolecular interaction energies of these optimized structures were calculated *via* the counterpoise method.[55] QM EDA data for different lanthanide–water dimers (Ln–H_2O) have been reported[56] and the results show that polarization energies contribute 54.0, 53.1, 52.4, and 51.1% of the total interaction energies of La^{3+}–H_2O, Eu^{3+}–H_2O, Gd^{3+}–H_2O, and Lu^{3+}–H_2O dimers, respectively. Those polarization contribution percentages enable us to estimate the polarization energies from the total QM interaction energy for other lanthanide–water dimers. In the AMOEBA model, polarization is described by the induction of a dipole on each interaction site. The induced dipole (μ_i) on each site i is calculated as $\mu_i = \alpha_i E_i$, where α_i is the atomic polarizability and E_i is the external electric field generated by the permanent multipoles or the induced dipoles on other sites. To avoid the so-called "polarization catastrophe", the dipole interactions are damped at short distances by using the Thole scheme.[57] The damped charge distribution in the AMOEBA force field[38] has the form $\rho = \frac{3a}{4\pi}\exp(-au^3)$, where $u = R_{ij}/(a_i a_j)^{1/6}$ is the effective distance as a function of the atomic polarizabilities of sites i and j, and a is a dimensionless parameter that controls the strength of damping. The parameter a was set to 0.39 in the water AMOEBA force field, but the values for divalent[37] and trivalent metal ions[30] should be reduced to obtain better descriptions of polarization energies for metal–water dimers (due to the small polarizabilities for these metal cations). Because the dipole polarizabilities (α) of the lanthanide ions have been reported,[58] we adjusted the damping parameters for lanthanide ions in this work to fit the AMOEBA polarization energy with the estimated polarization energies for different lanthanide–water dimers. The polarizability and damping factors for each lanthanide ion studied in this work are listed in Table 1.

In addition to Coulomb and polarization energies, the other type of AMOEBA intermolecular interaction of a lanthanide–water dimer corresponds to van der Waals interactions. These interactions are described by the buffered Halgren pairwise potential,[59]

$$U_{ij}^{\mathrm{vdW}} = \varepsilon_{ij}\left(\frac{1+0.07}{\left(\frac{r_{ij}}{R_{ij}^0}\right)+0.07}\right)^{14-7}\left(\frac{1+0.12}{\left(\frac{r_{ij}}{R_{ij}^0}\right)^7+0.12}-2\right)$$

Table 1 Polarizabilities (α), Thole damping exponents (a), and van der Waals parameters (R and ε) for Gd^{3+}, Dy^{3+}, and Ho^{3+}

Metal ions	α (Å^3)	a	R (Å)	ε (kcal mol^{-1})
Gd^{3+}	0.790[a]	0.146	3.30[b]	8.5[b]
Dy^{3+}	0.728[a]	0.140	3.23	15.0
Ho^{3+}	0.702[a]	0.136	3.20	20.0

[a] Ref. 58. [b] Ref. 30.

where ε_{ij} is a potential well (kcal mol^{-1}), r_{ij} is the separation distance between sites i and j, and R^0_{ij} is the minimum interaction energy distance (Å) for sites i and j. To describe the van der Waals interactions for different lanthanide–water dimers, the repulsion–dispersion parameters (R and ε in the Halgren function) for lanthanide ions were adjusted to match the remainder of the total interaction energy minus the sum of the AMOEBA coulomb and polarization energies. The resulting parameters for three lanthanide ions are listed in Table 1.

C. MD simulations procedure

Simulations of three lanthanide ions—Gd^{3+}, Dy^{3+}, and Ho^{3+}—were performed with two different liquid systems: water (system 1) and a mixture of water and [EMIm][$EtSO_4$] (1 : 19, v/v) (system 2). In water, the simulation of each lanthanide ion was performed with 511 water molecules, and the systems in water were tripositive. In system 2, 83 water molecules were placed randomly in a box of 150 [EMIm][$EtSO_4$] ion pairs because the volume ratio of water to [EMIm][$EtSO_4$] was 1 : 19, corresponding to the molar ratio of 83 : 150, to match the NMR experimental conditions.[34] For each lanthanide ion studied, three [EMIm] cations were replaced with a lanthanide ion in system 2 to keep the systems electroneutral. All simulations were performed using the AMBER12 package[60] and the AMOEBA polarizable force field with the above determined parameters. The simulations were carried out in an isothermal isobaric ensemble (*NPT*) at 298 K and 1 bar with a 1 fs time step using an 8.5 Å cutoff for non-bonded interactions and an 8.0 Å cutoff for the smooth particle mesh Ewald (PME) method[61] for long-range electrostatics. The Berendsen thermostat and barostat[62] were used to control the temperature and pressure with relaxation times of 1 and 3 ps, respectively. All production trajectories were generated for at least 10 ns, and snapshots were recorded every 100 fs. All properties such as the mean residence time were calculated from three independent MD trajectories with the standard deviation used as the uncertainty.

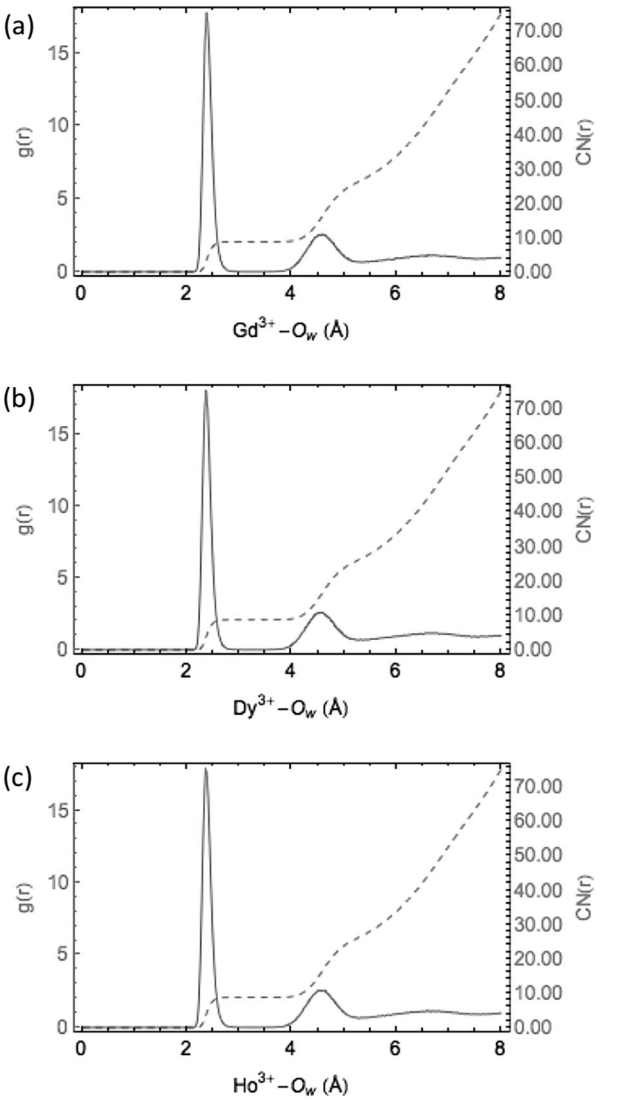

Fig. 1 Lanthanide–water oxygen (Ln–O_w) radial distribution functions (solid line) and the integration curves (CN(r), dashed line) for (a) Gd^{3+}, (b) Dy^{3+}, and (c) Ho^{3+}.

Results and discussion

The water-exchange rates of Gd^{3+}, Dy^{3+}, and Ho^{3+} in water as well as a water/[EMIm][$EtSO_4$] mixture were determined by ^{17}O-NMR experiments and have been reported previously.[25–27,34] In these two solvent systems, the lanthanide ions exhibited different trends in water-exchange rates. In water, water-exchange rates on lanthanide ions increase as a function of charge density (the ratio of charge to ionic radius). By contrast, lanthanide ions in water/[EMIm][$EtSO_4$] exhibited the opposite trend for the water-exchange rates, $Gd^{3+} < Dy^{3+} < Ho^{3+}$, moreover, the rates were also slower than in water alone. However, information about the reasons for these observed results was not easily accessible, and we suspected that MD simulations would provide atomic level insights to aid in the interpretation of these results.

Information about the structural properties at the atomic level of the three lanthanide ions in different solvent environments can be obtained from their radial distribution functions, $g(r)$. The $g(r)$ of the solvent molecules around each lanthanide ion in water and water/[EMIm][$EtSO_4$] is displayed in Fig. 1 and 2, respectively. In Fig. 1, the Ln–O_w $g(r)$ patterns are similar, and two well-resolved peaks indicate the location of the first and second hydration shells around the lanthanide ions. Table 2 shows that the position of the first Ln–O_w peak is dependent on the size of the specific ionic radius of the lanthanide ion. As the ionic radius decreases from Gd^{3+} to Ho^{3+}, the Ln–O_w distance decreases in the order of Gd^{3+}–O_w (2.38 Å) > Dy^{3+}–O_w (2.36 Å) > Ho^{3+}–O_w (2.35 Å). Integration of the first Ln–O_w $g(r)$ peak (dashed line in Fig. 1) represents the coordination numbers (CNs) of water molecules around each lanthanide ion in the first hydration shell, and the integrated values are listed in Table 2. The numbers of water molecules in the first hydration shell are between eight and nine due to water-exchange events between the first and the second shells.

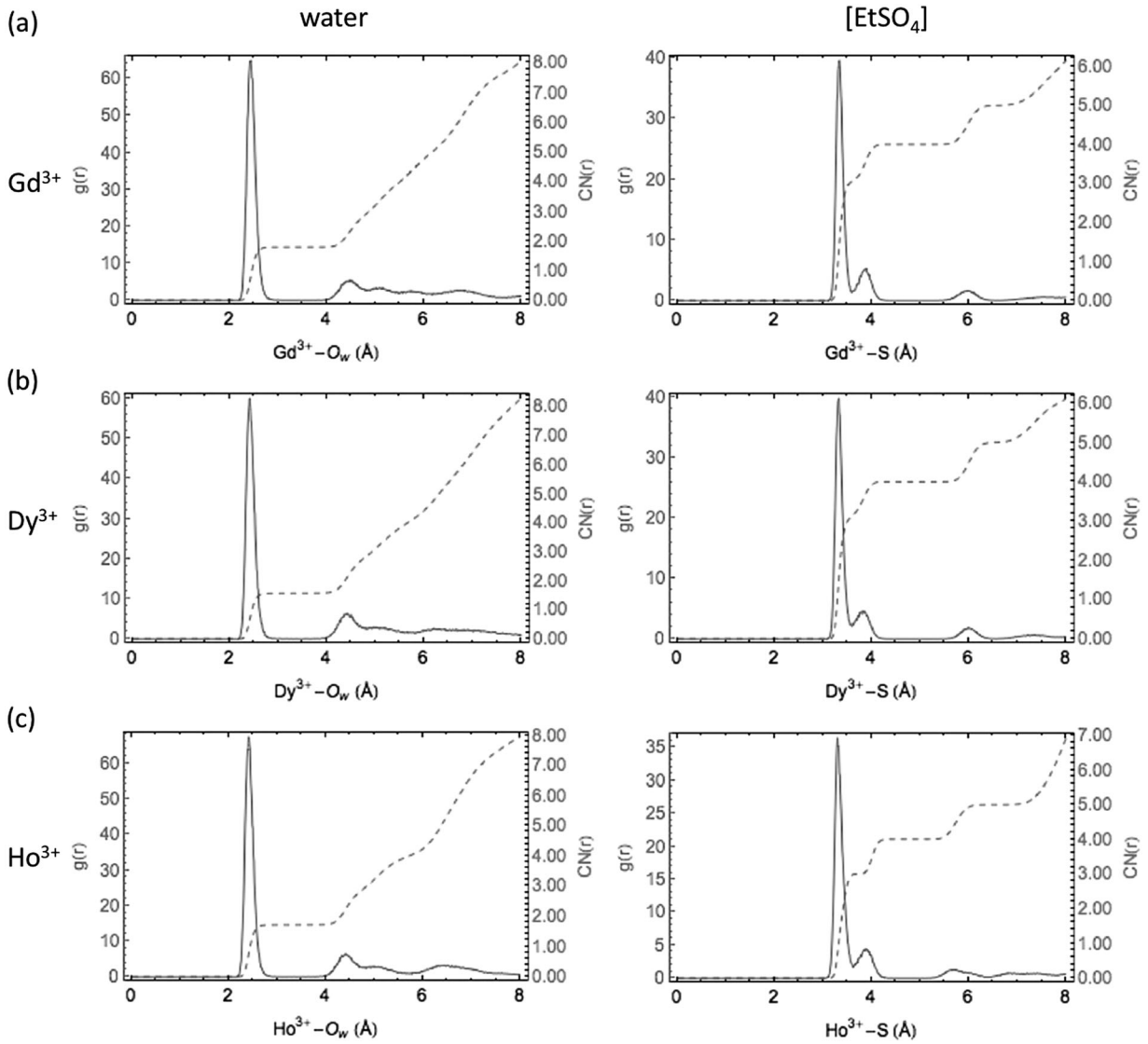

Fig. 2 Radial distribution functions and integration curves of water molecules (left panel) and $[EtSO_4]$ anions (right panel) around (a) Gd^{3+}, (b) Dy^{3+}, and (c) Ho^{3+} in water/[EMIm][$EtSO_4$].

Table 2 Coordination number (CN) and lanthanide–water distances ($Ln–O_w$) in the first hydration shell

Metal ions		Current work	Experiment[63]
Gd^{3+}	CN	8.8	8.7
	$Ln–O_w$	2.38	2.42
Dy^{3+}	CN	8.6	8.5
	$Ln–O_w$	2.36	2.38
Ho^{3+}	CN	8.7	8.4
	$Ln–O_w$	2.35	2.36

Table 3 Coordination number (CN) and lanthanide–water ($Ln–O_w$) and lanthanide–ethylsulfate (Ln–S)[a] distances in the first coordination shell from MD simulations (performed with 1 lanthanide ion + 147 $[EMIm]^+$ cations + 150 $[EtSO_4]^-$ anions + 83 water molecules)

$g(r)$	Metal ions	CN	Distance (Å)
$Ln–O_w$	Gd^{3+}	1.8	2.43
	Dy^{3+}	1.6	2.40
	Ho^{3+}	1.7	2.40
Ln–S	Gd^{3+}	(1) 3.0; (2) 1.0	(1) 3.33; (2) 3.84–3.88
	Dy^{3+}	(1) 3.0; (2) 1.0	(1) 3.32; (2) 3.81–3.85
	Ho^{3+}	(1) 3.0; (2) 1.0	(1) 3.29; (2) 3.84–3.87

[a] The first peak of Ln–S has two components: component (1) corresponds to three bidentate $[EtSO_4]^-$ anions and component (2) corresponds to one monodentate $[EtSO_4]^-$ anion.

In the water/[EMIm][$EtSO_4$] system, lanthanide ions can be surrounded by water and $[EtSO_4]^-$ anions, and the $Ln–O_w$ and Ln–S $g(r)$ in Fig. 2 display the distribution of the O atoms of water and the S atoms of $[EtSO_4]^-$ anions around each lanthanide ion, respectively. The positions of the first $g(r)$ peaks and the corresponding integral values (CN) are summarized in Table 3. Fig. 2 shows that the first peaks of the Ln–S $g(r)$ have two components. The one appearing at distances of 3.3–3.4 Å is associated with three bidentate $[EtSO_4]^-$ anions. The one located at a distance of 3.8–3.9 Å corresponds to $[EtSO_4]^-$ anions that

coordinate the metal ions in a monodentate fashion (Fig. 2, right panel). These data indicate that all three lanthanide ions are surrounded by four $[EtSO_4]^-$ anions in the first coordination shell.

When the size of the metal ions decreases from Gd^{3+} to Ho^{3+}, the distances of the first Ln–S peaks decrease as: Gd^{3+}–S (3.33 Å) > Dy^{3+}–S (3.32 Å) > Ho^{3+}–S (3.29 Å) (Fig. 2 and Table 3). In addition to $[EtSO_4]^-$ anions, the first coordination shell of the lanthanide ions also contains one or two water molecules due to water-exchange events. The distances of the first Ln–O_w $g(r)$ peaks are 2.43 Å for Gd^{3+}–O_w, 2.40 Å for Dy^{3+}–O_w, and 2.40 Å for Ho^{3+}–O_w, which are longer by 0.04–0.05 Å than those in pure water (2.38 Å for Gd^{3+}–O_w; 2.36 Å for Dy^{3+}–O_w; 2.35 Å for Ho^{3+}–O_w; see Table 2). The elongation of the Ln–O_w distance in water/[EMIm][$EtSO_4$] indicates that the presence of $[EtSO_4]^-$ weakens the interaction between the lanthanide ions and water molecules, potentially leading to differences in water dissociation rates and water exchanges.

Because molecular diffusion is one of the transport properties that is involved in water-exchange reactions, the prediction of diffusion coefficients can provide useful information for the kinetics of these chemical processes. The diffusion coefficients (D) of molecules can be determined by using the Einstein relation,[64]

$$6Dt = \lim_{t\to\infty} \mathrm{MSD}(t)$$

where MSD is the mean-square displacement over a period of time (t). In the diffusive regime, MSD grows linearly with time, so the diffusion coefficient can be calculated from the slope of the plot of MSD as a function of time.

To investigate the effect of solvents on molecular diffusion, the diffusion coefficients of water (D_{H_2O}) and each lanthanide ion (D_{Ln}, Ln = Gd^{3+}, Dy^{3+}, or Ho^{3+}) in water were calculated from the slopes of MSD plots (see the ESI†) and compared to the corresponding values in water/[EMIm][$EtSO_4$]. Table 4 shows that the diffusion coefficients of water (D_{H_2O}) are in the range of 1.59×10^{-5}–1.63×10^{-5} $cm^2\ s^{-1}$ in water and 7.86×10^{-9}–1.40×10^{-8} $cm^2\ s^{-1}$ in water/[EMIm][$EtSO_4$]. The self-diffusivities of water in water/[EMIm][$EtSO_4$] are smaller than those in water because the diffusion coefficients of $[EtSO_4]^-$ anions are in the range of 2.99×10^{-9}–4.28×10^{-9} $cm^2\ s^{-1}$ in water/[EMIm][$EtSO_4$], and water molecules form strong hydrogen bonds with the $[EtSO_4]^-$ anions. These hydrogen bonds restrain the motion of water and lead to slower dynamics in water/[EMIm][$EtSO_4$].

Table 4 Self-diffusion coefficients for water (D_{H_2O}) and lanthanide ions (D_{Ln}) and in water and [EMIm][$EtSO_4$][a]

Solvent	Metal ions	D_{H_2O} ($cm^2\ s^{-1}$)	D_{Ln} ($cm^2\ s^{-1}$)	D_{EtSO_4} ($cm^2\ s^{-1}$)
Water	Gd^{3+}	1.62×10^{-5}	1.04×10^{-5}	
Water	Dy^{3+}	1.63×10^{-5}	1.78×10^{-6}	
Water	Ho^{3+}	1.59×10^{-5}	8.11×10^{-7}	
Water/[EMIm][$EtSO_4$]	Gd^{3+}	1.40×10^{-8}	1.65×10^{-10}	4.28×10^{-9}
Water/[EMIm][$EtSO_4$]	Dy^{3+}	8.64×10^{-9}	1.80×10^{-10}	3.10×10^{-9}
Water/[EMIm][$EtSO_4$]	Ho^{3+}	7.86×10^{-9}	3.37×10^{-10}	2.99×10^{-9}

[a] The standard deviation from three independent MD simulations are provided in the ESI.

A similar solvent effect can be observed in the diffusion coefficients of lanthanide ions (D_{Ln}) in these two solvent systems. Table 4 shows that diffusion coefficients for Gd^{3+}, Dy^{3+}, and Ho^{3+} are 1.65×10^{-10}, 1.80×10^{-10}, and 3.37×10^{-10} $cm^2\ s^{-1}$, respectively, in water/[EMIm][$EtSO_4$], but these coefficients are slower than the rates in water (1.04×10^{-5} $cm^2\ s^{-1}$ for Gd^{3+}, 1.78×10^{-6} $cm^2\ s^{-1}$ for Dy^{3+}, and 8.11×10^{-7} $cm^2\ s^{-1}$ for Ho^{3+}). In part, the slower diffusion rates of lanthanide ions in water/[EMIm][$EtSO_4$] are because the electrostatic interactions of lanthanide ions with $[EtSO_4]^-$ anions are stronger than with neutral water molecules and because the water molecules coordinated to lanthanide ions are bridged by the surrounding $[EtSO_4]^-$ *via* ionic hydrogen bonds. The molecular diffusions for water and lanthanide ions in water/[EMIm][$EtSO_4$] being slower than those in water is consistent with the ^{17}O-NMR experimental results demonstrating that the water-exchange rates of lanthanide ions are slower in water/[EMIm][$EtSO_4$] than in water.

To study the size effect of metal ions on their mobility, the diffusion coefficient of each lanthanide ion was determined in a given solvent system. In water/[EMIm][$EtSO_4$], all studied lanthanide ions have similar diffusion rates. In water, on the other hand, the diffusion rates of the lanthanide ions decrease as a function of their ionic radii.[65] The calculated diffusion coefficients are 1.04×10^{-5} $cm^2\ s^{-1}$ for Gd^{3+}, 1.78×10^{-6} $cm^2\ s^{-1}$ for Dy^{3+}, and 8.11×10^{-7} $cm^2\ s^{-1}$ for Ho^{3+}. This trend is because the larger lanthanide ions with lower charge densities bind to solvent molecules less tightly than smaller ions with higher charge densities, causing faster dynamics. Experiments found that the water-exchange rate decreases from Gd^{3+} to Ho^{3+} in water.[25–27]

To determine the water-exchange rate (k_{ex}), we calculated the averaged residence time ($\tau = 1/k_{ex}$) of a water molecule in the first solvation shell using the following equation for $R(t)$:[66]

$$R(t) = \left\langle \frac{1}{N_0} \sum_{i=1}^{N_0} P_i(t, t^*) \right\rangle$$

where N_0 is the total number of water molecules in the first hydration shell of the lanthanide ion at time $t = 0$. $P_i(t,t^*)$ is the time correlation function, which takes a value of 1 if the water molecule i continuously stays in the first shell between time 0 and time t, or if the water molecule leaves the first hydration shell within t^*; otherwise, $P_i(t,t^*)$ is 0. In this work, the parameter t^* is taken to be 2 ps in water and 100 ps in water/[EMIm][$EtSO_4$] due to the smaller mobility of molecules in this solvent. The distance of a water molecule within the first hydration shell is defined as Ln–O_w < 3.25 Å from Ln–O_w $g(r)$. The function $R(t)$ decays exponentially with respect to time t, and the mean residence time of a water molecule around a lanthanide ion (τ) can be obtained by fitting an exponential form ($e^{-t/\tau}$) to $R(t)$. The calculated water-exchange rates (k_{ex}) and the inverse of the mean residence time are shown in Table 5 and Fig. 3.

In water, the calculated water-exchange rates are 1.30×10^9, 7.72×10^8, and 4.75×10^8 s^{-1} for Gd^{3+}, Dy^{3+}, and Ho^{3+}, respectively. The water-exchange rates exhibit the trend of

Table 5 Water-exchange rates (k_{ex}, s^{-1}) for lanthanide ions in water or water/[EMIm][$EtSO_4$]

Solvent	Metal ions	Current work	Experiments[26,27,34]
Water	Gd^{3+}	1.30×10^9	$8.30 \times 10^{8\,a}$
Water	Dy^{3+}	7.72×10^8	$4.34 \times 10^{8\,b}$
Water	Ho^{3+}	4.75×10^8	$2.14 \times 10^{8\,b}$
Water/[EMIm][$EtSO_4$]	Gd^{3+}	2.96×10^7	$5.08 \times 10^{6\,c}$
Water/[EMIm][$EtSO_4$]	Dy^{3+}	4.94×10^7	$3.64 \times 10^{7\,c}$
Water/[EMIm][$EtSO_4$]	Ho^{3+}	8.86×10^7	$4.61 \times 10^{7\,c}$

[a] Ref. 27. [b] Ref. 26. [c] Ref. 34.

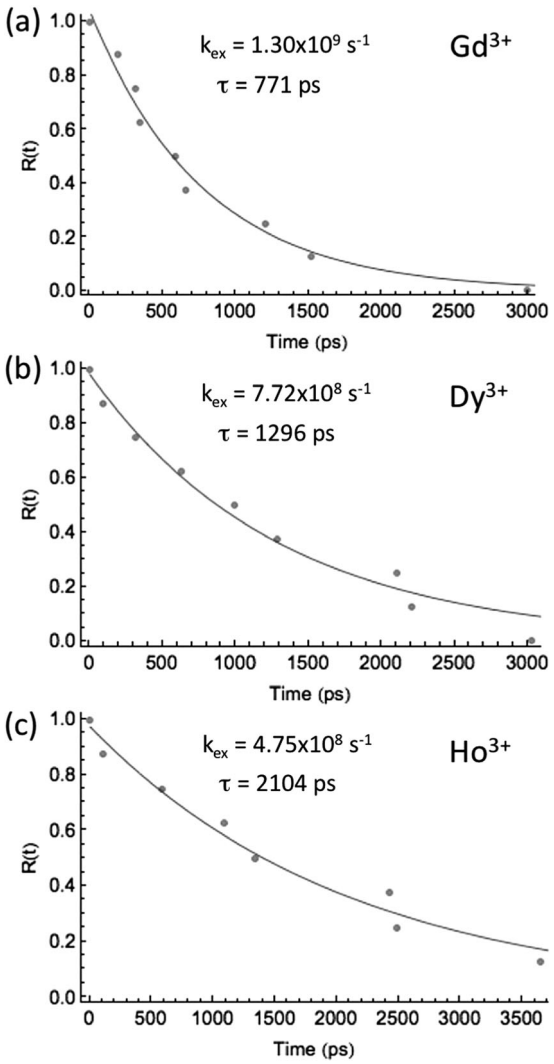

Fig. 3 Residence probability $R(t)$ that a particular water molecule stays in the first hydration shell of (a) Gd^{3+}, (b) Dy^{3+}, and (c) Ho^{3+} after a correlation time for the simulations in water.

$Gd^{3+} > Dy^{3+} > Ho^{3+}$. In water/[EMIm][$EtSO_4$], the water-exchange rates are 2.96×10^7 s^{-1} for Gd^{3+}, 4.94×10^7 s^{-1} for Dy^{3+}, and 8.86×10^7 s^{-1} for Ho^{3+}, which are slower than the rates for the same ions in water. In addition, the trend of the water-exchange rates is the opposite to that in water. The calculated water-exchange rates given in Table 5 are faster than the experimental measurements;[25–27,34] nevertheless, the trends in the two solvent systems are consistent with the ^{17}O-NMR experiments.

A water-exchange event can be viewed in terms of the time difference between a water molecule coming into the first shell and another water molecule leaving the first shell. Based on solvent substitutions along different reaction coordinates, water-exchange mechanisms can be classified as (1) an associative path where an incoming water joins the first coordination sphere in the first step; (2) a dissociative path where an outgoing water leaves the first solvation shell in the first step; and (3) an interexchange process where the outgoing water comes out from the first shell at the same time as the entering water joins the first shell.[67]

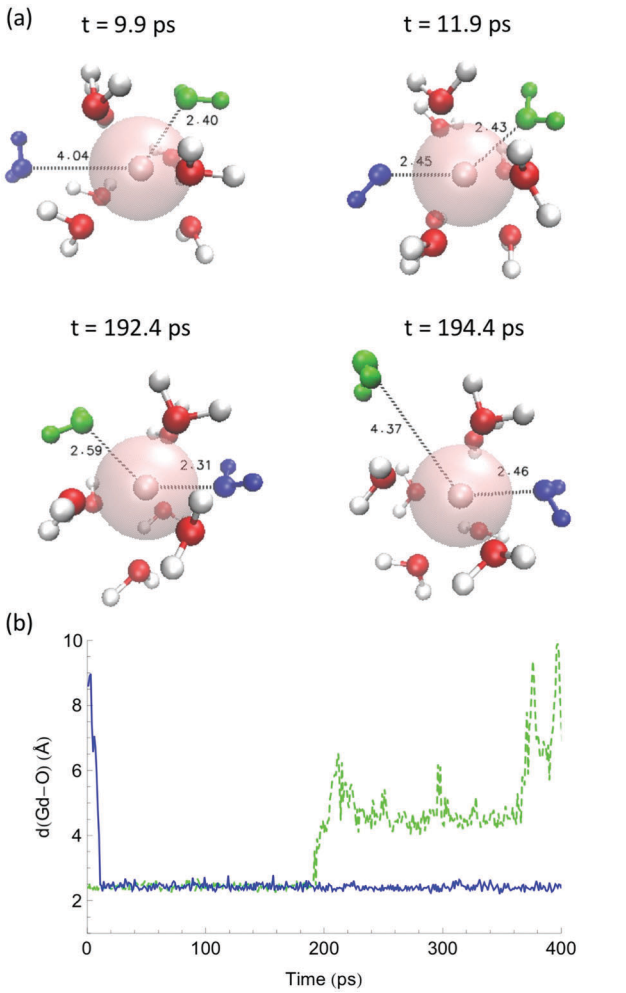

Fig. 4 (a) MD snapshots for a water-exchange event on Gd^{3+}. The water molecules colored in blue and green represent the incoming and outgoing water molecules, respectively. At t = 9.9 ps, there are eight water molecules in the first hydration shell of Gd^{3+}. Between 11.9 and 192.2 ps, the ninth water molecule (blue) from the bulk joins the first coordination shell, characteristic of an associative mechanism. At t = 194.4 ps, the green water molecule has moved out of the first hydration shell and the blue water molecule stays in the first hydration shell. (b) The corresponding trajectory for the water exchange observed in (a). The blue solid and green dashed trajectories represent the incoming and outgoing water molecules, respectively.

By analyzing the lanthanide–oxygen distance and snapshots from MD trajectories, we can observe the transitions of water-exchange events between the first coordination shell and the bulk along the distance trajectories and have a qualitative picture to distinguish these solvent exchange processes in different solvent systems. Fig. 4(a) shows selected snapshots for the water exchange of Gd^{3+} in water. A similar behavior is observed for Dy^{3+} and Ho^{3+} in water. At the beginning of the simulation (t = 0 ps in Fig. 4(a)), the first hydration shell of Gd^{3+} has eight water molecules, forming a square antiprism (SAP) geometry. During the simulation, one water molecule from the bulk joins the first hydration shell, and a nine-coordinate lanthanide aquo complex is formed with a tricapped trigonal prism (TTP) geometry. Subsequently, when a water molecule is released from the first shell to the outer hydration shells, the remaining eight water molecules in the first shell rearrange themselves to the SAP geometry. Fig. 4(b) shows that the lanthanide–water distance trajectories for the incoming and outgoing water molecules overlap at the distance of the first hydration shell, which suggests that lanthanide ions employ an associative pathway for water exchange in water. To initiate water exchange in water, a water molecule from the bulk must move into the first shell. The ionic radii of lanthanide ions have two main effects on the water association process.[26] First, the smaller lanthanide ions with higher charge density can result in faster association of water molecules. On the other hand, to provide room for one additional water molecule in the first shell, the SAP structure for the eight-coordinate lanthanide aquo complex must rearrange itself into a bicapped trigonal prism (BTP) so that the incoming water molecule can attack one of the square faces of the initial SAP structure to form the TTP structure for the nine-coordinate aquo complex. Because the ionic radii of lanthanide ions are in the order of Gd^{3+} > Dy^{3+} > Ho^{3+}, the smaller lanthanide ions form smaller aquo complexes with the surrounding water molecules, resulting in smaller square faces of the SAP structures. The smaller square face makes it less accessible for the incoming water to join the first shell of the lanthanide ion, preventing the association of the incoming water from the bulk. Therefore, a decreasing trend of Gd^{3+} > Dy^{3+} > Ho^{3+} is observed for the water-exchange rates in water.

When the water-exchange processes of lanthanide ions were simulated in water/[EMIm][$EtSO_4$], the beginning MD snapshot (t = 0 ps in Fig. 5(b)) shows that Ho^{3+} binds with nine O atoms from four $[EtSO_4]^-$ anions and two water molecules in the first coordination shell. In addition, the Ho^{3+} ion slightly deviates from the S1–S2–S3 plane (see the definition of ϕ(S1–S2–S3–Ho^{3+}) in Fig. 5(a)) by 24.2 degrees at t = 0 ps. During the first few nanoseconds of MD simulations, no exchanges of water or other ligands were observed. Nevertheless, we observed that the $[EtSO_4]^-$ anions underwent rapid spin motions around the lanthanide ion. In some occasions, these rotational motions cause the central lanthanide ion to deviate from the S1–S2–S3 plane and elongate the lanthanide–water distance, preventing the binding of the first shell water to the lanthanide ion. When the ϕ(S1–S2–S3–Ho^{3+}) torsion angle is increased from the average of 28.6 degrees to the average of 37.5 degrees (right panel in Fig. 6(a)), the average distance of the lanthanide–water oxygen is elongated from 2.46 to 4.72 Å, indicating the dissociation of a water molecule from the first coordination shell. When a first-shell water molecule is lost, water exchange is imminent. The entering water can be the original outgoing water from the first

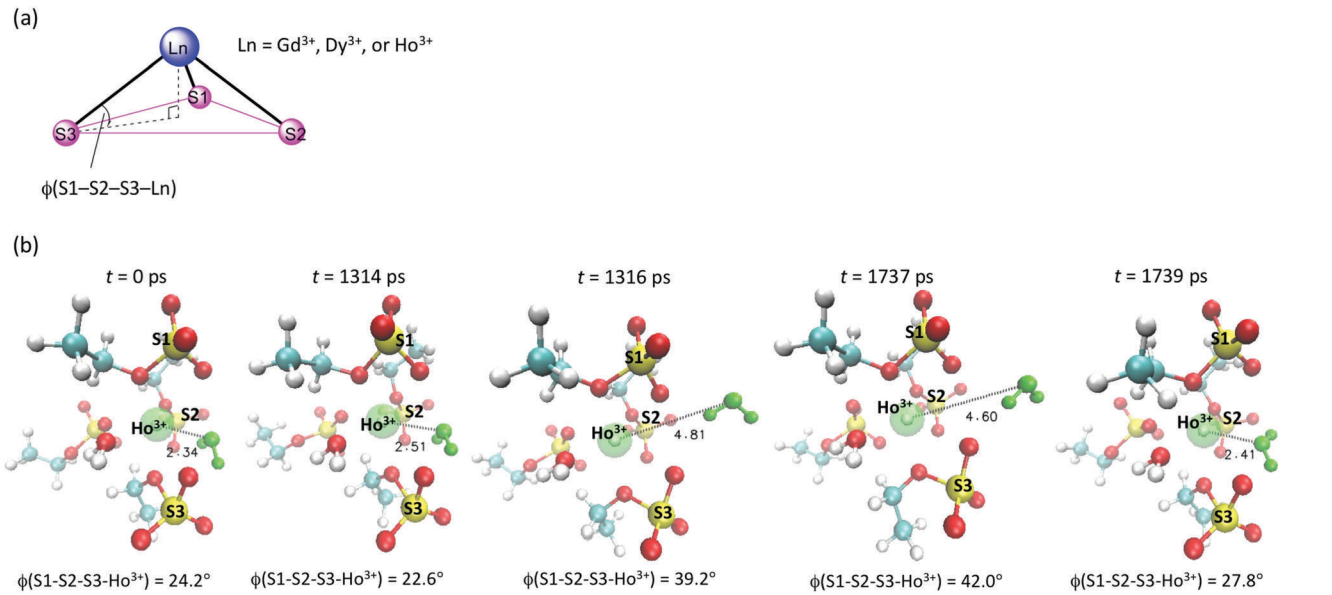

Fig. 5 (a) The definition of dihedral angle ϕ(S1–S2–S3–Ln): a lanthanide ion deviates from the S1–S2–S3 plane by ϕ(S1–S2–S3–Ln). (b) MD snapshots for a water-exchange event around Ho^{3+} in water//[EMIm][$EtSO_4$]. From t = 0 to 1.314 ps, Ho^{3+} forms a 9-coordinate complex with $[EtSO_4]^-$ anions and water molecules in the first coordination shell. The green water molecule leaves the first coordination sphere at 1.316 ps and stays in the second or the third coordination spheres until 1.737 ps. The green water joins the first solvation shell again at 1.739 ps, and a water exchange is complete. This reaction follows a dissociative pathway.

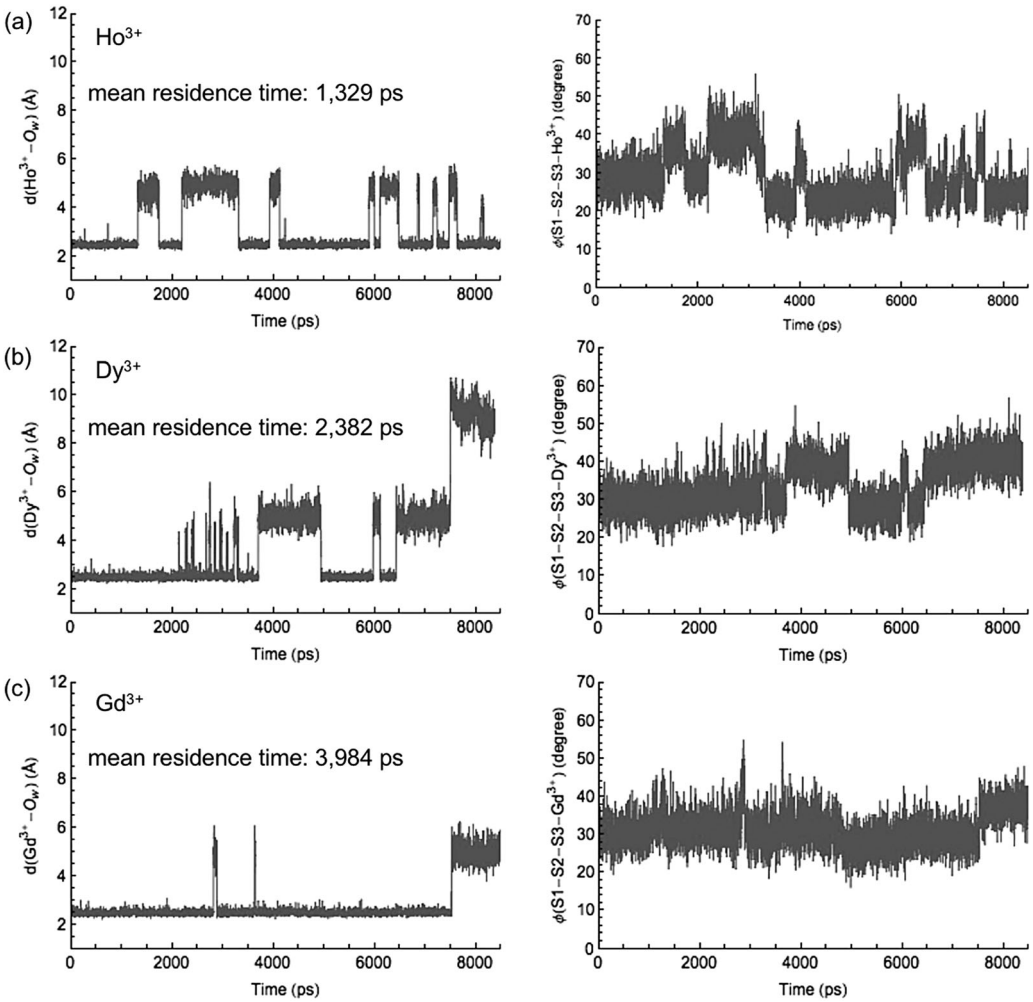

Fig. 6 The distance of lanthanide–water oxygen (left panel) and the dihedral angle ϕ(S1–S2–S3–Ln) (right panel) over simulation time demonstrating the time when a water molecule travels between the first and outer coordination spheres of (a) Ho^{3+}, (b) Dy^{3+}, and (c) Gd^{3+} in water/[EMIm][$EtSO_4$]. Other independent trajectories are provided in the ESI.†

shell or other water molecules from the outer-sphere. Similar behaviors were observed for Dy^{3+} and Gd^{3+} in water/[EMIm][$EtSO_4$] (Fig. 6(b) and (c)).

Fig. 6 shows the time required to dissociate a water molecule from the first solvation shell for the three studied lanthanide ions. For the dissociation of a water molecule, the average time it took was 1.329 ps for Ho^{3+}, 2.382 ps for Dy^{3+}, and 3.984 ps for Gd^{3+}. The residence time of a water in the first shell is in the order of $Ho^{3+} < Dy^{3+} < Gd^{3+}$ and is dependent on the charge density of the lanthanide ion that influences the electrostatic interactions between the lanthanide cation and the $[EtSO_4]^-$ anions. As shown in the Ln–S $g(r)$ plots, the $[EtSO_4]^-$ anions bind more tightly to Ho^{3+} than Gd^{3+} due to the smaller ionic radius of Ho^{3+}. As a result, the first coordination shell of Ho^{3+} is sterically more crowded than Gd^{3+}, hindering the binding of water to the lanthanide and resulting in water molecules being released more easily from Ho^{3+} than from Gd^{3+}. These results likely explain why the experiments found that water-exchange rates in water/[EMIm][$EtSO_4$] appeared in the order of $Gd^{3+} < Dy^{3+} < Ho^{3+}$. Interestingly, no water-exchange event was observed for these lanthanide ions throughout all MD trajectories when the simulations of the water-exchange reactions were started from the configuration where two first shell water molecules were adjacent to each other (Fig. 7). This type of solvent configuration might provide insight for ligand design for manipulation of water-exchange rates in future experiments.

Conclusions

Experiments have shown that the water-exchange rates of lanthanide ions can be manipulated by choosing different solvents and metal ions. In water, the water-exchange rate decreases in the order of $Gd^{3+} > Dy^{3+} > Ho^{3+}$. By contrast, the inverse trend, $Gd^{3+} < Dy^{3+} < Ho^{3+}$, is observed in water/[EMIm][$EtSO_4$]. To gain further insight into these water-exchange events, we developed AMOEBA parameters for the [EMIm][$EtSO_4$] ion pair as well as the corresponding lanthanide ions and performed classical MD simulations with these new parameters. By analyzing the MD trajectories, we calculated the

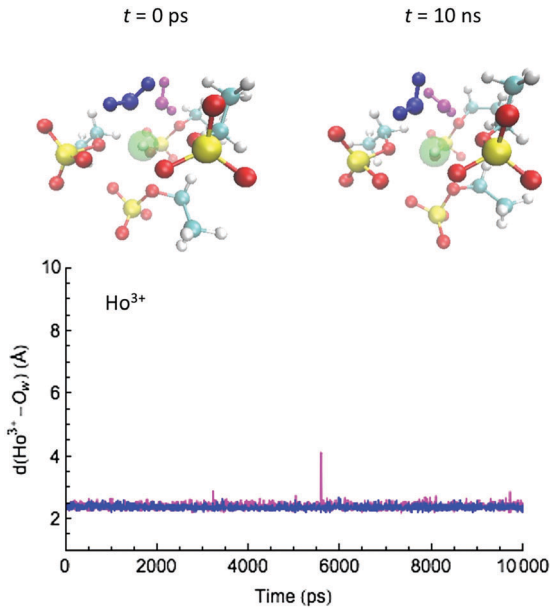

Fig. 7 MD snapshots and lanthanide–water oxygen distance trajectories showing that no water-exchange event was observed throughout the entire simulation time when two water molecules (blue and pink) were adjacent to each other in the first solvation shell of Ho^{3+}. Similar behaviors were observed for Gd^{3+} and Dy^{3+}.

water-exchange rates of lanthanide ions in water and water/[EMIm][$EtSO_4$] and analyzed the interactions between the lanthanide ions with water molecules and [EMIm][$EtSO_4$]. Our simulations are in agreement with experimental results with respect to water-exchange trends. Furthermore, the atomic-level insight of our simulations indicates that in water, the water-exchange events follow an associative process. The water-exchange rate of Ho^{3+} being slower than that of Gd^{3+} might be explained by stronger electrostatic interactions with the first shell water of Ho^{3+} due to its smaller ionic radius compared to Gd^{3+}, preventing the association of water with the first shell. On the other hand, water exchange in water/[EMIm][$EtSO_4$] is initiated by dissociating a water molecule from the first shell. The residence time of the first shell water depends on the relative binding strength of the lanthanide ion with $[EtSO_4]^-$ anions and water molecules. The first shell $[EtSO_4]^-$ binds to the smaller lanthanide ions more tightly and causes more steric effects on the first shell water molecules, facilitating the dissociation of water. As a result, the trend of $Gd^{3+} < Dy^{3+} < Ho^{3+}$ is seen for the water-exchange rates in water/[EMIm][$EtSO_4$]. This study shows how the interactions between metal ions and solvents influence the water-exchange rates and provides guidance for the selection of suitable solvents and metals for optimizing water-exchange rates.

Acknowledgements

This work was supported by Wayne State University. Y.-J. T. thanks WSU for a Rumble Fellowship. The authors thank the Wayne State University Grid for computing time.

References

1 S. Tang, A. Babai and A. V. Mudring, Europium-based ionic liquids as luminescent soft materials, *Angew. Chem., Int. Ed.*, 2008, **47**, 7631–7634.
2 P. Dissanayake and M. J. Allen, Dynamic Measurements of Aqueous Lanthanide Triflate-Catalyzed Reactions Using Luminescence Decay, *J. Am. Chem. Soc.*, 2009, **131**, 6342–6343.
3 A. de Bettencourt-Dias, P. S. Barber and S. Bauer, A Water-Soluble Pybox Derivative and Its Highly Luminescent Lanthanide Ion Complexes, *J. Am. Chem. Soc.*, 2012, **134**, 6987–6994.
4 A. Foucault-Collet, K. A. Gogick, K. A. White, S. Villette, A. Pallier, G. Collet, C. Kieda, T. Li, S. J. Geib and N. L. Rosi, *et al.*, Lanthanide near infrared imaging in living cells with Yb3+ nano metal organic frameworks, *Proc. Natl. Acad. Sci. U. S. A.*, 2013, **110**, 17199–17204.
5 A. N. W. Kuda-Wedagedara, C. C. Wang, P. D. Martin and M. J. Allen, Aqueous Eu-II-Containing Complex with Bright Yellow Luminescence, *J. Am. Chem. Soc.*, 2015, **137**, 4960–4963.
6 B. Mallick, B. Balke, C. Felser and A. V. Mudring, Dysprosium room-temperature ionic liquids with strong luminescence and response to magnetic fields, *Angew. Chem., Int. Ed.*, 2008, **47**, 7635–7638.
7 J. D. Rinehart, M. Fang, W. J. Evans and J. R. Long, Strong exchange and magnetic blocking in *N*-2(3-)-radical-bridged lanthanide complexes, *Nat. Chem.*, 2011, **3**, 538–542.
8 L. Ungur, J. J. Le Roy, I. Korobkov, M. Murugesu and L. F. Chibotaru, Fine-tuning the Local Symmetry to Attain Record Blocking Temperature and Magnetic Remanence in a Single-Ion Magnet, *Angew. Chem., Int. Ed.*, 2014, **53**, 4413–4417.
9 L. A. Ekanger, L. A. Polin, Y. Shen, E. M. Haacke, P. D. Martin and M. J. Allen, A Eu-II-Containing Cryptate as a Redox Sensor in Magnetic Resonance Imaging of Living Tissue, *Angew. Chem., Int. Ed.*, 2015, **54**, 14398–14401.
10 C. E. Song, W. H. Shim, E. J. Roh and J. H. Choi, Scandium(III) triflate immobilised in ionic liquids: a novel and recyclable catalytic system for Friedel–Crafts alkylation of aromatic compounds with alkenes, *Chem. Commun.*, 2000, 1695–1696.
11 M. Shibasaki and N. Yoshikawa, Lanthanide complexes in multifunctional asymmetric catalysis, *Chem. Rev.*, 2002, **102**, 2187–2209.
12 J. R. Robinson, X. Y. Fan, J. Yadav, P. J. Carroll, A. J. Wooten, M. A. Pericas, E. J. Schelter and P. J. Walsh, Air- and Water-Tolerant Rare Earth Guanidinium BINOLate Complexes as Practical Precatalysts in Multifunctional Asymmetric Catalysis, *J. Am. Chem. Soc.*, 2014, **136**, 8034–8041.
13 Y. J. Mei, D. J. Averill and M. J. Allen, Study of the Lanthanide-Catalyzed, Aqueous, Asymmetric Mukaiyama Aldol Reaction, *J. Org. Chem.*, 2012, **77**, 5624–5632.
14 S. Kobayashi, S. Nagayama and T. Busujima, Lewis acid catalysts stable in water. Correlation between catalytic activity in water and hydrolysis constants and exchange rate constants for substitution of inner-sphere water ligands, *J. Am. Chem. Soc.*, 1998, **120**, 8287–8288.

15 B. N. Siriwardena-Mahanama and M. J. Allen, Strategies for Optimizing Water-Exchange Rates of Lanthanide-Based Contrast Agents for Magnetic Resonance Imaging, *Molecules*, 2013, **18**, 9352–9381.
16 B. A. Rosen, A. Salehi-Khojin, M. R. Thorson, W. Zhu, D. T. Whipple, P. J. A. Kenis and R. I. Masel, Ionic Liquid-Mediated Selective Conversion of CO2 to CO at Low Overpotentials, *Science*, 2011, **334**, 643–644.
17 Q. H. Zhang, S. G. Zhang and Y. Q. Deng, Recent advances in ionic liquid catalysis, *Green Chem.*, 2011, **13**, 2619–2637.
18 A. C. Atesin, N. A. Ray, P. C. Stair and T. J. Marks, Etheric C-O Bond Hydrogenolysis Using a Tandem Lanthanide Triflate/Supported Palladium Nanoparticle Catalyst System, *J. Am. Chem. Soc.*, 2012, **134**, 14682–14685.
19 M. J. Schneider, M. Haumann and P. Wasserscheid, Asymmetric hydrogenation of methyl pyruvate in the continuous gas phase using Supported Ionic Liquid Phase (SILP) catalysis, *J. Mol. Catal. A: Chem.*, 2013, **376**, 103–110.
20 W. S. Miao and T. H. Chan, Ionic-liquid-supported synthesis: A novel liquid-phase strategy for organic synthesis, *Acc. Chem. Res.*, 2006, **39**, 897–908.
21 J. P. Hallett and T. Welton, Room-Temperature Ionic Liquids: Solvents for Synthesis and Catalysis. 2, *Chem. Rev.*, 2011, **111**, 3508–3576.
22 T. Vander Hoogerstraete, S. Wellens, K. Verachtert and K. Binnemans, Removal of transition metals from rare earths by solvent extraction with an undiluted phosphonium ionic liquid: separations relevant to rare-earth magnet recycling, *Green Chem.*, 2013, **15**, 919–927.
23 A. Chaumont and G. Wipff, Solvation of M3+ lanthanide cations in room-temperature ionic liquids. A molecular dynamics investigation, *Phys. Chem. Chem. Phys.*, 2003, **5**, 3481–3488.
24 E. Bodo, Lanthanum(III) and Lutetium(III) in Nitrate-Based Ionic Liquids: A Theoretical Study of Their Coordination Shell, *J. Phys. Chem. B*, 2015, **119**, 11833–11838.
25 C. Cossy, L. Helm and A. E. Merbach, O-17 Nuclear Magnetic-Resonance Kinetic-Study of Water Exchange on the Lanthanide(III) Aqua Ions, *Inorg. Chem.*, 1988, **27**, 1973–1979.
26 C. Cossy, L. Helm and A. E. Merbach, High-Pressure NMR-Study Water-Exchange Mechanisms on the Terbium to Thulium Octaaqualanthanide(III) Ions – a Variable-Pressure O-17 NMR-Study, *Inorg. Chem.*, 1989, **28**, 2699–2703.
27 K. Micskei, D. H. Powell, L. Helm, E. Brucher and A. E. Merbach, Water Exchange on $[Gd(H_2O)(8)](3+)$ and $[Gd(Pdta)(H_2O)(2)](-)$ in Aqueous-Solution - a Variable-Pressure, Variable-Temperature and Variable-Magnetic Field O-17 Nmr-Study, *Magn. Reson. Chem.*, 1993, **31**, 1011–1020.
28 C. Clavaguera, R. Pollet, J. M. Soudan, V. Brenner and J. P. Dognon, Molecular dynamics study of the hydration of lanthanum(III) and europium(III) including many-body effects, *J. Phys. Chem. B*, 2005, **109**, 7614–7616.
29 C. Clavaguera, F. Calvo and J. P. Dognon, Theoretical study of the hydrated Gd3+ ion: Structure, dynamics, and charge transfer, *J. Chem. Phys.*, 2006, **124**, 074505.
30 A. Marjolin, C. Gourlaouen, C. Clavaguera, P. Y. Y. Ren, J. P. Piquemal and J. P. Dognon, Hydration gibbs free energies of open and closed shell trivalent lanthanide and actinide cations from polarizable molecular dynamics, *J. Mol. Model.*, 2014, **20**, 2471.
31 R. Dessapt, L. Helm and A. E. Merbach, DMSO exchange on [Gd(DMSO)(8)](3+) – a variable pressure O-17 NMR study, *J. Phys.: Condens. Matter*, 2004, **16**, S1027–S1032.
32 S. F. Lincoln and A. White, Ligand-Exchange on Hexakis-(1,1,3,3-Tetramethylurea) Complexes of Trivalent Lanthanides – Proton Nuclear-Magnetic-Resonance Study, *Inorg. Chim. Acta*, 1990, **168**, 265–270.
33 D. L. Pisaniello, L. Helm, P. Meier and A. E. Merbach, High pressure NMR kinetics. 19. Variable pressure and temperature nuclear magnetic resonance and visible spectrophotometric studies of lanthanide ions in dimethylformamide: solvation and solvent exchange dynamics, *J. Am. Chem. Soc.*, 1983, **105**, 4528–4536.
34 Z. Lin, M. L. Shelby, D. Hayes, K. A. Fransted, L. X. Chen and M. J. Allen, Water-exchange rates of lanthanide ions in an ionic liquid, *Dalton Trans.*, 2014, **43**, 16156–16159.
35 C. Clavaguera-Sarrio, V. Brenner, S. Hoyau, C. J. Marsden, P. Millie and J. P. Dognon, Modeling of uranyl cation-water clusters, *J. Phys. Chem. B*, 2003, **107**, 3051–3060.
36 A. Marjolin, C. Gourlaouen, C. Clavaguera, P. Y. Y. Ren, J. C. Wu, N. Gresh, J. P. Dognon and J. P. Piquemal, Toward accurate solvation dynamics of lanthanides and actinides in water using polarizable force fields: from gas-phase energetics to hydration free energies, *Theor. Chem. Acc.*, 2012, **131**, 1198.
37 J. P. Piquemal, L. Perera, G. A. Cisneros, P. Y. Ren, L. G. Pedersen and T. A. Darden, Towards accurate solvation dynamics of divalent cations in water using the polarizable amoeba force field: From energetics to structure, *J. Chem. Phys.*, 2006, **125**, 054511.
38 P. Y. Ren and J. W. Ponder, Polarizable atomic multipole water model for molecular mechanics simulation, *J. Phys. Chem. B*, 2003, **107**, 5933–5947.
39 J. C. Wu, J. P. Piquemal, R. Chaudret, P. Reinhardt and P. Y. Ren, Polarizable Molecular Dynamics Simulation of Zn(II) in Water Using the AMOEBA Force Field, *J. Chem. Theory Comput.*, 2010, **6**, 2059–2070.
40 G. A. Cisneros, Application of Gaussian Electrostatic Model (GEM) Distributed Multipoles in the AMOEBA Force Field, *J. Chem. Theory Comput.*, 2012, **8**, 5072–5080.
41 O. N. Starovoytov, H. Torabifard and G. A. Cisneros, Development of AMOEBA force field for 1,3-dimethylimidazolium based ionic liquids, *J. Phys. Chem. B*, 2014, **118**, 7156–7166.
42 K. Kitaura and K. Morokuma, A New Energy Decomposition Scheme for Molecular-Interactions within the Hartree-Fock Approximation, *Int. J. Quantum Chem.*, 1976, **10**, 325–340.
43 E. Gomez, B. Gonzalez, N. Calvar, E. Tojo and A. Dominguez, Physical properties of pure 1-ethyl-3-methylimidazolium ethylsulfate and its binary mixtures with ethanol and water at several temperatures, *J. Chem. Eng. Data*, 2006, **51**, 2096–2102.

44 J. P. Armstrong, C. Hurst, R. G. Jones, P. Licence, K. R. J. Lovelock, C. J. Satterley and I. J. Villar-Garcia, Vapourisation of ionic liquids, *Phys. Chem. Chem. Phys.*, 2007, **9**, 982–990.

45 D. H. Zaitsau, K. Fumino, V. N. Emel'yanenko, A. V. Yermalayeu, R. Ludwig and S. P. Verevkin, Structure-Property Relationships in Ionic Liquids: A Study of the Anion Dependence in Vaporization Enthalpies of Imidazolium-Based Ionic Liquids, *ChemPhysChem*, 2012, **13**, 1868–1876.

46 M. J. Frisch, M. Head-Gordon and J. A. Pople, A Direct MP2 Gradient-Method, *Chem. Phys. Lett.*, 1990, **166**, 275–280.

47 M. J. Frisch, M. Head-Gordon and J. A. Pople, Semi-direct Algorithms for the MP2 Energy and Gradient, *Chem. Phys. Lett.*, 1990, **166**, 281–289.

48 M. Head-Gordon, J. A. Pople and M. J. Frisch, MP2 Energy Evaluation by Direct Methods, *Chem. Phys. Lett.*, 1988, **153**, 503–506.

49 M. Head-Gordon and T. Head-Gordon, Analytic MP2 Frequencies without 5th-Order Storage: Theory and Application to Bifurcated Hydrogen-Bonds in the Water Hexamer, *Chem. Phys. Lett.*, 1994, **220**, 122–128.

50 S. Saebo and J. Almlof, Avoiding the Integral Storage Bottleneck in LCAO Calculations of Electron Correlation, *Chem. Phys. Lett.*, 1989, **154**, 83–89.

51 M. J. Frisch, G. W. Trucks, H. B. Schlegel, G. E. Scuseria, M. A. Robb, J. R. Cheeseman, G. B. V. Scalmani, B. Mennucci, G. A. Petersson and H. Nakatsuji, *et al.*, Gaussian Development Version, Revision H.35, Gaussian, Inc., Wallingford CT, 2014, Complete citation in the ESI†.

52 A. Bergner, M. Dolg, W. Kuchle, H. Stoll and H. Preuss, Ab-Initio Energy-Adjusted Pseudopotentials for Elements of Groups 13-17, *Mol. Phys.*, 1993, **80**, 1431–1441.

53 M. Dolg, H. Stoll, H. Preuss and R. M. Pitzer, Relativistic and Correlation Effects for Element 105 (Hahnium, Ha) - a Comparative-Study of M and MO (M = Nb, Ta, Ha) Using Energy-Adjusted ab Initio Pseudopotentials, *J. Phys. Chem.*, 1993, **97**, 5852–5859.

54 M. Kaupp, P. V. Schleyer, H. Stoll and H. Preuss, Pseudopotential Approaches to Ca, Sr, and Ba Hydrides – Why Are Some Alkaline-Earth MX2 Compounds Bent?, *J. Chem. Phys.*, 1991, **94**, 1360–1366.

55 W. J. Stevens and W. H. Fink, Frozen Fragment Reduced Variational Space Analysis of Hydrogen-Bonding Interactions – Application to the Water Dimer, *Chem. Phys. Lett.*, 1987, **139**, 15–22.

56 A. Marjolin, C. Gourlaouen, C. Clavaguera, J. P. Dognon and J. P. Piquemal, Towards energy decomposition analysis for open and closed shell f-elements mono aqua complexes, *Chem. Phys. Lett.*, 2013, **563**, 25–29.

57 B. T. Thole, Molecular Polarizabilities Calculated with a Modified Dipole Interaction, *Chem. Phys.*, 1981, **59**, 341–350.

58 C. Clavaguera and J. P. Dognon, Accurate static electric dipole polarizability calculations of +3 charged lanthanide ions, *Chem. Phys.*, 2005, **311**, 169–176.

59 T. A. Halgren, Representation of Vanderwaals (vdW) Interactions in Molecular Mechanics Force-Fields – Potential Form, Combination Rules, and Vdw Parameters, *J. Am. Chem. Soc.*, 1992, **114**, 7827–7843.

60 D. A. Case, T. A. Darden, T. E. Cheatham III, C. L. Simmerling, J. Wang, R. E. Duke, R. Luo, R. C. Walker, W. Zhang and K. M. Merz, *et al.*, AMBER 12, University of California, San Francisco, CA, 2012, Complete citation in the ESI†.

61 T. Darden, L. Perera, L. P. Li and L. Pedersen, New tricks for modelers from the crystallography toolkit: the particle mesh Ewald algorithm and its use in nucleic acid simulations, *Structure*, 1999, **7**, R55–R60.

62 H. J. C. Berendsen, J. P. M. Postma, W. F. Vangunsteren, A. Dinola and J. R. Haak, Molecular-Dynamics with Coupling to an External Bath, *J. Chem. Phys.*, 1984, **81**, 3684–3690.

63 P. R. Smirnov and V. N. Trostin, Structural parameters of the nearest surrounding of lanthanide ions in aqueous solutions of their salts, *Russ. J. Gen. Chem.*, 2012, **82**, 360–378.

64 M. P. Allen and D. J. Tildesley, *Computer Simulations of Liquids*, Oxford University Press, New York, 1987.

65 E. Mauerhofer, K. Zhernosekov and F. Rosch, Limiting transport properties of lanthanide and actinide ions in pure water, *Radiochim. Acta*, 2003, **91**, 473–477.

66 R. W. Impey, P. A. Madden and I. R. Mcdonald, Hydration and Mobility of Ions in Solution, *J. Phys. Chem.*, 1983, **87**, 5071–5083.

67 C. H. Langford and H. B. Gray, *Ligand Substitution Processes*, W. A. Benjamin, Inc., New York, 1966.